# Rotational Diffusion of Calcium-Dependent Adenosine-5′-triphosphatase in Sarcoplasmic Reticulum: A Detailed Study†

Colin J. Restall, Robert E. Dale, Elaine K. Murray, Charles W. Gilbert, and Dennis Chapman*

ABSTRACT: The $Ca^{2+}$–$Mg^{2+}$ adenosine-5′-triphosphatase (ATPase) in sarcoplasmic reticulum has been covalently labeled with the phosphorescent triplet probe erythrosinyl 5-isothiocyanate. The rotational diffusion of the protein in the membrane at 25 °C was examined by measuring the time dependence of the phosphorescence emission anisotropy. Detailed analysis of both the total emission $S(t) = I_V(t) + 2I_H(t)$ and anisotropy $R(t) = [I_V(t) - I_H(t)]/[I_V(t) + 2I_H(t)]$ curves shows the presence of multiple components. The latter is incompatible with a simple model of protein movement. The experimental data are consistent with a model in which the sum of four exponential components defines the phosphorescence decay. The anisotropy decay corresponds to a model in which the phosphor itself or a small phosphor-bearing segment reorients on a sub-microsecond time scale about an axis attached to a larger segment, which in turn reorients on a time scale of a few microseconds about an axis fixed in the frame of the ATPase. A fraction of the protein molecules rotate on a time scale of 100–200 μs about the normal to the bilayer, while the rest are rotationally stationary, at least on a sub-millisecond time scale.

Modern studies of biological membranes have shown that the dynamics and degree of order of the membrane components need to be carefully considered in order to understand how a biomembrane functions in vivo (Chapman & Restall, 1982). The investigation of membrane protein rotational diffusion is normally performed by optical spectroscopy or saturation transfer EPR[1] [see Cherry (1979) for review]. In the absence of a suitable intrinsic chromophore, the optical techniques rely on adsorbing or covalently linking a triplet probe such as eosin or erythrosin to the protein of interest. Excitation of the bound triplet probe by a brief polarized laser flash results in dichroic singlet absorption and polarized triplet emission. The lifetime of the triplet state is long lived, and it allows micro- to millisecond relaxation times to be measured.

Other studies, both in our own laboratory (Hoffmann et al., 1979, 1980; Restall et al., 1981) and elsewhere (Kirino et al., 1978; Thomas & Hidalgo, 1978; Burkli & Cherry, 1981; Thomas et al., 1982; Speirs et al., 1983), have shown that the ($Ca^{2+}$–$Mg^{2+}$)ATPase from sarcoplasmic reticulum exhibits rotational movement on the micro- to millisecond time scale both in its natural membrane and in fluid-reconstituted systems. Furthermore, the evidence suggests that an environmental condition that allows this movement, or possibly rotational freedom per se, is necessary for the biological activity of the protein. It has been shown (Restall et al., 1981; Burkli & Cherry, 1981; Speirs et al., 1983) that the rotational diffusion of this protein is complex and appears to be consistent with binding of the probe to a rapidly reorienting polypeptide segment of the protein, which itself rotates as a whole in the effectively stationary membrane. In the present paper, the results of a detailed analysis of polarized phosphorescence decay data for ($Ca^{2+}$–$Mg^{2+}$)ATPase labeled with erythrosinyl 5-isothiocyanate in situ in purified sarcoplasmic reticulum are detailed. Mathematical models for the various molecular movements are described and were applied in the analyses in which iterative nonlinear least-squares curve fitting procedures were used in order to establish and quantitate the model of minimal complexity consistent with the experimental results.

## Theory

In the model of a labeled protein embedded in a phospholipid bilayer, illustrated in Figure 1, the phosphorescent probe is assumed to be covalently bound to a segment of the protein. The absorption transition moment $\vec{\mu}_a$ and emission transition moment $\vec{\mu}_e$ of the phosphor make fixed angles $\theta_a$ and $\theta_e$, respectively, with an axis $\vec{p}$ fixed in this segment. This axis is envisaged as undergoing restricted Brownian rotational diffusion about an axis of 3-fold or higher symmetry $\vec{m}$, fixed in the protein. The protein as a whole undergoes one-dimensional rotational motion about the axis $\vec{n}$ normal to the lipid bilayer. By extension of the general argument first put forward by Steiner and McAlister in 1957 [see also Kawato & Kinosita (1981)], the phosphorescence anisotropy decay can be described by the product of the ensemble-averaged depolarization factors of these independent motions as follows:

$$r(t) = 0.4\left(\frac{3}{2}\langle[\vec{\mu}_a(0)\cdot\vec{\mu}_e(t)]^2\rangle - \frac{1}{2}\right) = 0.4\left(\frac{3}{2}\langle\cos^2\lambda_p(t)\rangle - \frac{1}{2}\right)\left(\frac{3}{2}\langle\cos^2\lambda_m(t)\rangle - \frac{1}{2}\right) \quad (1)$$

The first ensemble-averaged depolarization factor results from the reorientation $\lambda_p(t)$ between the absorption moment $\vec{\mu}_a$ at the instant of excitation and the emission moment $\vec{\mu}_e$ at time $t$ when the emission occurs, relative to the coordinate frame of the axis $\vec{m}$, i.e., to a stationary $\vec{m}$. The second term describes the reorientation $\lambda_m(t)$ of $\vec{m}$ relative to the membrane, which is assumed to be immobile in the laboratory frame.

The phosphorescence anisotropy decay due to the independent rotations of a series of $k$ successive segments between

† From the Department of Biochemistry and Chemistry, Royal Free Hospital School of Medicine, London NW3 2PF, U.K. (C.J.R., E.K.M., and D.C.), and Paterson Laboratories, Christie Hospital and Holt Radium Institute, Manchester M20 9BX, U.K. (R.E.D. and C.W.G.). *Received November 17, 1983; revised manuscript received June 1, 1984.* This work was supported by The Muscular Dystrophy Group of Great Britain, The Science and Engineering Research Council, The Cancer Research Campaign, The Wellcome Trust, and The Royal Society.

[1] Abbreviations: ATPase, adenosine-5′-triphosphatase; EPR, electron paramagnetic resonance; $NaDodSO_4$, sodium dodecyl sulfate; Tris-HCl, tris(hydroxymethyl)aminomethane hydrochloride.

0006-2960/84/0423-6765$01.50/0 

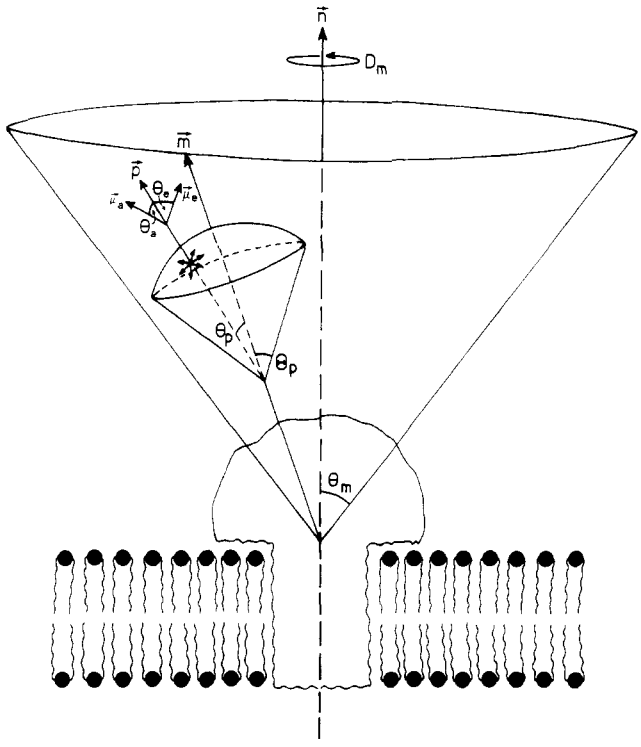


FIGURE 1: Schematic diagram of a simple model of the ($Ca^{2+}$–$Mg^{2+}$)ATPase from sarcoplasmic reticulum indicating the geometrical relationships between the absorption and emission transition moments $\vec{\mu}_a$ and $\vec{\mu}_e$ of the phosphor, the axis $\vec{p}$ of the segment to which it is attached, the axis $\vec{m}$ about which $\vec{p}$ diffuses, fixed in the protein as a whole, and the bilayer normal, $\vec{n}$. The reorientational relaxation processes are pictured as being symmetric about the successive axes.

the primary attachment site of the phosphor and the motion of the protein as a whole is described by

$$r(t) = 0.4\left(\frac{3}{2}\langle\cos^2\lambda_p(t)\rangle - \frac{1}{2}\right) \times \left[\prod_{s=1}^{k}\left(\frac{3}{2}\langle\cos^2\lambda_s(t)\rangle - \frac{1}{2}\right)\right]\left(\frac{3}{2}\langle\cos^2\lambda_m(t)\rangle - \frac{1}{2}\right) \quad (2)$$

For example, if there is one intermediary segment about whose axis $\vec{s}$ the segment containing $\vec{\mu}_a$ and $\vec{\mu}_e$ reorients (i.e., whose axis $\vec{s}$ is an axis of symmetry for the restricted rotational motion of $\vec{p}$) and which itself reorients about axis $\vec{m}$, eq 2 becomes

$$r(t) = 0.4\left(\frac{3}{2}\langle\cos^2\lambda_p(t)\rangle - \frac{1}{2}\right)\left(\frac{3}{2}\langle\cos^2\lambda_s(t)\rangle - \frac{1}{2}\right) \times \left(\frac{3}{2}\langle\cos^2\lambda_m(t)\rangle - \frac{1}{2}\right) \quad (3)$$

The term in $\cos\lambda_m(t)$, which refers to one-dimensional free rotation of the vector $\vec{m}$ about the bilayer normal $\vec{n}$ with which it makes angle $\theta_m$, can be accurately established by the Steiner and McAlister approach [see Dale & Eisinger (1975)]. If $\delta(t)$ is defined as the azimuth swept out by $\vec{m}$ in time $t$, corresponding to the change in orientation $\lambda_m(t)$ of $\vec{m}$, the cosine rule relates $\theta_m$, $\delta(t)$, and $\lambda_m(t)$ by

$$\cos\lambda_m(t) = \cos^2\theta_m + \sin^2\theta_m\cos[\pm\delta(t)] \quad (4)$$

Substituting this into the depolarization factor arising from rotation of $\vec{m}$ leads, after squaring, averaging, and rearranging, to

$$\frac{3}{2}\langle\cos^2\lambda_m(t)\rangle - \frac{1}{2} = \frac{3}{4}\sin^4\theta_m\,(2\langle\cos^2\delta(t)\rangle - 1) + 3\cos^2\theta_m\sin^2\theta_m\,\langle\cos\delta(t)\rangle + \left(\frac{3}{2}\cos^2\theta_m - \frac{1}{2}\right)^2 \quad (5)$$

The averages of the functions of $\delta(t)$ can be expressed in terms of the one-dimensional rotational diffusion coefficient $D_m$, leading to

$$\frac{3}{2}\langle\cos^2\lambda_m(t)\rangle - \frac{1}{2} = B_{m1}\exp(-4D_m t) + B_{m2}\exp(-D_m t) + B_{m3} \quad (6)$$

where

$$B_{m1} + B_{m2} + B_{m3} = 1 \quad (7)$$

corresponding to the result of Gottlieb & Wahl (1963) for one-dimensional rotation of a fluorophore-bearing segment on a macromolecule in the limit that the macromolecular substrate is stationary.

A similar treatment could be applied to $\langle\cos^2\lambda_s(t)\rangle$ and $\langle\cos^2\lambda_p(t)\rangle$, the latter resulting in more complex forms of the coefficients [e.g., Dale & Eisinger (1975)], but the one-dimensional rotational model is almost certainly inappropriate in these cases. It is much more reasonable to consider a model in which $\vec{s}$ has Brownian rotational freedom within some orientational distribution that is radially symmetrical about $\vec{m}$, such as the "wobbling-in-a-cone" model (Kinosita et al., 1977), and the reorientation of $\vec{p}$ about $\vec{s}$ may be considered similarly.

The form of the depolarization factors for various reorientation models has been examined by a number of workers (Kinosita et al., 1977, 1982; Lipari & Szabo, 1980; Zannoni, 1981) and may be written as

$$\frac{3}{2}\langle\cos^2\lambda(t)\rangle - \frac{1}{2} = [\sum_n B_n\exp(-t/\phi_n)] + B_\infty \quad (8)$$

$B_n$, $\phi_n$, and $B_\infty$ are, at least in principle, explicitly definable in terms of the specific model invoked. The time-dependent sum may be well-approximated in many cases by a small number of exponential terms $\sum_j B_j\exp(-t/\phi_j)$, whose weights $B_j$ and correlation times $\phi_j$ are weighted averages of the true $B_n$ and $\phi_n$.

The constant $B_\infty$ can be expressed in model-independent form. Thus, the depolarization factor for reorientation of the axis $\vec{p}$ about $\vec{s}$ is given by

$$\frac{3}{2}\langle\cos^2\lambda_p(t)\rangle - \frac{1}{2} = [\sum_j B_{pj}\exp(-t/\phi_{pj})] + B_{p\infty} \quad (9)$$

with

$$B_{p\infty} = \left(\frac{3}{2}\cos^2\theta_a - \frac{1}{2}\right)\left(\frac{3}{2}\cos^2\theta_e - \frac{1}{2}\right)\left(\frac{3}{2}\langle\cos^2\theta_p\rangle - \frac{1}{2}\right)^2 \quad (10)$$

where

$$\langle\cos^2\theta_p\rangle = \left[\int_{\theta_p} f(\theta_p)\cos^2\theta_p\sin\theta_p\,d\theta_p\right]\Big/\left[\int_{\theta_p} f(\theta_p)\sin\theta_p\,d\theta_p\right] \quad (11)$$

in which $f(\theta_p)$ is the radial probability density of the equilibrium orientation of $\vec{p}$ about $\vec{s}$; e.g., $f(\theta_p) = 1$ for $0 < \theta_p < \Theta_p$ in the wobbling-in-a-cone model, $\Theta_p$ being the half-cone angle. In addition

$$\sum_j B_{pj} + B_{p\infty} = \left(\frac{3}{2}\cos^2\theta_{ae} - \frac{1}{2}\right)\left(\frac{3}{2}\langle\cos^2\theta_p\rangle - \frac{1}{2}\right)^2 \quad (12)$$

where $\theta_{ae}$ is the angle between the absorption and emission vectors in the molecular frame of the phosphor. The depolarization arising from the reorientation of axis $\vec{s}$ about $\vec{m}$ is simpler:

$$\frac{3}{2}\langle\cos^2\lambda_s(t)\rangle - \frac{1}{2} = \sum_{j'} B_{sj'}\exp(-t/\phi_{sj'}) + B_{s\infty} \quad (13)$$

with

$$B_{s\infty} = \left(\frac{3}{2}\langle\cos^2\theta_s\rangle - \frac{1}{2}\right)^2 \quad (14)$$

where $\langle\cos^2\theta_s\rangle$ is defined by the equilibrium orientational distribution of $\vec{s}$ about $\vec{m}$ in the equivalent of eq 11 and

$$\sum_{j'} B_{sj'} + B_{s\infty} = 1 \quad (15)$$

Overall, by use of the shorthand Legendre polynomial representation

$$P_2(\cos\alpha) = \frac{3}{2}\cos^2\alpha - \frac{1}{2} \quad (16)$$

the time-dependence of the phosphorescence emission anisotropy is thus given by

$$r(t) = 0.4[\sum_j B_{pj}\exp(-t/\phi_{pj}) + P_2(\cos\theta_a)P_2(\cos\theta_e) \times \langle P_2(\cos\theta_p)\rangle^2][\sum_{j'} B_{sj'}\exp(-t/\phi_{sj'}) + \langle P_2(\cos\theta_s)\rangle^2] \times [B_{m1}\exp(-4D_m t) + B_{m2}\exp(-D_m t) + P_2^2(\cos\theta_m)] \quad (17)$$

The critical assumptions made in this derivation are that successive segmental reorientational relaxation processes give rise at each stage to equilibrium orientational distributions of the vectors concerned and that these are radially symmetric with respect to a vector associated with the substrate on which this reorientation occurs, i.e., $\vec{a}$, $\vec{e}$, and $\vec{p}$ about $\vec{s}$, $\vec{s}$ about $\vec{m}$, and $\vec{m}$ about $\vec{n}$, the last being fixed in the laboratory coordinate frame.

## Materials and Methods

*Preparation of Sarcoplasmic Reticulum.* Sarcoplasmic reticulum vesicles were prepared from the back and hind leg white muscles of rabbit as described elsewhere (Gomez-Fernandez et al., 1980). The material so obtained was purified by centrifuging it through a 20–60% w/v continuous sucrose density gradient containing 1 M KCl, 5 mM $Mg^{2+}$-ATP, 2 mM dithiothreitol, and 50 mM Tris-HCl, pH 8.0, before use. After purification, the vesicles were stored frozen at −20 °C.

*Labeling with Erythrosinyl Isothiocyanate.* Erythrosinyl 5-isothiocyanate (Molecular Probes Inc., Junction City, OR 97448) was dissolved in 50 mM sodium phosphate buffer, pH 8.0, at a concentration of approximately 0.5 mg/mL. The extinction coefficient of erythrosinyl isothiocyanate was assumed to be the same as that for eosinyl isothiocyanate for their respective maxima at 530 and 522 nm ($8.3 \times 10^4$ $M^{-1}$ $cm^{-1}$) (Cherry et al., 1976; Garland & Moore, 1979). This value was then used to calculate the true concentration of erythrosin present in solution.

Labeling of the purified sarcoplasmic reticulum was performed by incubating the protein with an equimolar amount of probe solution in 50 mM sodium phosphate buffer, pH 8.0, for 1 h in the dark. All the manipulations were made under dim red illumination (Kodak Safelight filter No. 1) in order to prevent photooxidative damage to the protein (Restall et al., 1981; Burkli & Cherry, 1981). Upon completion of the incubation, the reticulum was sedimented by centrifuging it at 100000*g* for 30 min at 4 °C and then resuspended at a concentration of about 0.5–0.7 mg/mL in 50 mM sodium phosphate buffer, pH 8.0, containing 66% v/v glycerol. In order to prevent oxygen quenching of the phosphorescence, samples were flushed with nitrogen prior to performing the flash photolysis measurements.

*Phosphorescence Polarization Measurements.* The sample of erythrosin-labeled sarcoplasmic reticulum in a glass cuvette was excited by a 20-ns, plane-polarized laser flash at 530 nm, generated by a J. K. Laser System 2000, fitted with a KD*P frequency-doubling crystal. The laser-induced phosphorescence was collected from both sides of the sample cuvette, perpendicular to the direction of the laser beam, and focussed through polarizers (type 03 FPG 001, Melles Griot, Arnhem, Holland) aligned parallel on one side and perpendicular on the other side to the electric vector of the laser excitation. This was oriented in the vertical direction normal to the plane of excitation and observation, yielding signals $I_{VV}(t)$ and $I_{HV}(t)$, respectively. The orthogonally polarized phosphorescence components were detected with photomultipliers (R928 from Hamamatsu Ltd.) through red-pass filters (6-mm Schott glass RG645 and 3-mm RG655, Barr and Stroud Ltd., Glasgow). After amplification, the decay signals were captured in a Datalab DL1080 transient recorder and averaged in a DL4000 signal averager (Data Laboratories Ltd., Mitcham, Surrey).

After the desired number of signals (typically 64 or 128) was collected, the averaged data were transferred to a Sharp MZ80B desktop computer. Collection of these data sets was alternated with that of the same two emission components excited by horizontally polarized radiation produced by appropriate reorientation of the laser half-wave plate accessory. The collection of these two components [$I_{HV}(t)$ and $I_{HH}(t)$] was essential to allow correction for differences in the efficiency of registration of the orthogonally polarized emission components.[2]

To check for the absence of significant instrumental depolarization effects (Steinberg, 1975), the fluorescence anisotropy of $5 \times 10^{-6}$ M fluorescein in 95% (v/v) aqueous glycerol containing 0.1 N NaOH [exciting with a tungsten light source via a Grubb-Parsons filter ($\lambda_{max}$ = 473 nm, FWHM = 14 nm) and observing the emission via a Schott cutoff filter transmitting beyond 515 nm] was measured to be $\langle r\rangle = 0.333 \pm 0.002$ compared with the literature value for this system of $0.378 \pm 0.002$, corresponding to $\langle p\rangle = 0.477 \pm 0.002$ (Chen & Bowman, 1965). Depolarizing effects of scatter (Teale, 1969) are eliminated in the present sarcoplasmic reticulum due to the close matching of refractive indexes of the membrane materials by the solvent containing 66% v/v glycerol.

*Data Reduction and Analysis.* From symmetry considerations, $I_{HV}(t)$ and $I_{HH}(t)$ are ideally identical, and their ratio is independent of both the decay of the excited-state population and its depolarization. It turns out experimentally in the present system that not only are these components slightly different on average (this difference being minimized by adjusting the photomultiplier gains in the two arms) but their ratio $G(t) = I_{HH}(t)/I_{HV}(t)$ also exhibits small but significant variations with time on the time scales of both the decay (about $10^{-3}$ s) and the alternation of data collection (about $10^3$ s), as indicated in the upper panel of Figure 2. The source of this time variation has not been located, but on application of the ratio to correct the relative values of $I_{VV}(t)$ and $I_{VH}(t)$, consistent experimental phosphorescence anisotropy decays $R(t)$ defined by

$$R(t) = [I_{VV}(t)G(t) - I_{VH}(t)]/S(t) \quad (18)$$

with consistent experimental phosphorescence decays $S(t)$ defined by

$$S(t) = I_{VV}(t)G(t) + 2I_{VH}(t) \quad (19)$$

were in general obtainable. Maverick (VV, VH) or (HV, HH) data sets that appeared from time to time in an alternating

[2] The convention of using upper case to designate data ($I$, $S$, $R$) and lower case for theoretical and calculated functions ($i$, $s$, $r$) is adopted.

collection sequence of 4 × (HV, HH), 3 × (VV, VH) were rejected after inspection of $R(t)$ curves, which are much more sensitive to $G(t)$ variations than are the $S(t)$ curves. These were produced from each (VV, VH) data set by correction with $G(t)$ curves produced from (a) (HV, HH) sets collected immediately before, (b) those collected immediately after, and (c) the sums of these two sets. The $I_{VV}(t)G(t)$ and $I_{HV}(t)$ data sets giving consistent $R(t)$ curves, judged as smoothed curves differing from each other by not more than about ±0.002 over their whole time range, were then summed to produce data sets for analysis.

The first few microseconds of data were distorted by overloading of the photomultipliers apparently by the "initial" burst of prompt fluorescence registered even at the much longer wavelengths of phosphorescence selected by the filter, possibly in combination with filter fluorescence activated by the prompt erythrosin emission. However, it was demonstrated with equivalent suspensions of unlabeled sarcoplasmic reticulum and with aqueous solutions of erythrosinyl isothiocyanate at comparable concentrations to those present in the labeled ATPase suspensions that recovery to base line was complete by 5 μs. Phosphorescence data prior to this time was therefore rejected in all cases, setting a lower limit of approximately 2-μs resolution in the analysis of decay times.

Data sets produced as above were analyzed by a NAG (Nottingham Algorithm Group) library modified Marquardt iterative nonlinear least-squares subroutine (Fletcher, 1971) in an Algol vector anisotropy analysis program (Gilbert, 1983) developed for the CDC 7600 system of the University of Manchester Regional Computer Centre (UMRCC). In this analysis procedure, the fitting of calculated mono- or multiexponential time-courses $s(t)$ and $r(t)$

$$s(t) = \sum_i \alpha_i \exp(-t/\tau_i) \tag{20}$$

$$r(t) = \sum_j \beta_j \exp(-t/\phi_j) \tag{21}$$

($\alpha_i$ representing the initial intensity of the decay component $i$ having a lifetime $\tau_i$; $\beta_j$ the partial anisotropy of component $j$ associated with rotational correlation time $\phi_j$), to $i_{VV}(t)$ and $i_{VH}(t)$, now taken to be fully corrected, according to

$$i_{VV}(t) = [s(t)/3][1 + 2r(t)] \tag{22}$$

and

$$i_{VH}(t) = [s(t)/3][1 - r(t)] \tag{23}$$

is carried out simultaneously. The significance of the different decay components $i$ and $j$ depends on the models considered for the excited-state decay kinetics and rotational depolarization. Some of these models require particular values of, or relationships between, $\beta_j$ values or $\phi_j$ values or both, and this is also catered for by allowing any of these values or the ratios of any two or more of them to be fixed during the analysis. The search routine looks for a minimum of the sum of squares of unweighted residuals ($\chi^2$) between calculated and experimental curves and terminates when no variable in the search changes from its value at the previous iteration by more than $10^{-6}$ (the variables used are $\alpha_i$, $\kappa_i = \tau_i^{-1}$, and $\gamma_j = \phi^{-1}$ in units of reciprocal channels and $\beta_j$, which is dimensionless).

In the absence of an absolute theoretical weighting function for this kind of data, unweighted residuals were opted for on the basis of inspection of the $G(t)$ curves in which the noise level across the decay range concerned of about 0.5 ms is fairly constant (Figure 2). This was subsequently supported by the relative uniformity of the differences between the best fitting theoretical functions and the data (q.v.).

Straightforward analyses in terms of mono- and multiexponential models of $s(t)$ and $r(t)$ without additional restrictions were initially carried out. This was to obtain reasonable estimates for the initial values of the anisotropy decay variables in the particular rotational models considered and to help establish the minimal complexity of the model giving an adequate fit between the calculated and experimental curves. The quality of the agreement was determined by consideration of the comparative values of the sums of squared residuals for different models and by their randomness of distribution. In each analysis, standard deviations for the variables and combinations of them were obtained from the variance and covariance estimates given in the error matrix produced at the final iteration.

## Results

*Probe Location.* In contrast to studies of protein rotational diffusion utilizing intrinsic chromophores, such as bacteriorhodopsin, the use of extrinsic triplet probes raises several questions, the first of which concerns their location. It seems highly probable that the major binding site for the probe is the ($Ca^{2+}$–$Mg^{2+}$)ATPase since the sarcoplasmic reticulum membrane contains predominantly this protein (Malan et al., 1975). The only additional protein that is partially exposed to the external surface is the high-affinity calcium binding protein, which is only present in small amounts (Sarzala & Michalak, 1978) and which has been reported not to react preferentially with the related probe eosinyl isothiocyanate (Hoffmann et al., 1979).

It is important, however, to exclude the possibility that an appreciable fraction of the probe is bound to the lipid molecules. Consequently, excess chloroform–methanol (2:1 v/v) was added to a sample of the labeled sarcoplasmic reticulum, and after a thorough mixing, sufficient water was added to form a two-phase system in which the lipids are partitioned into the lower organic layer while any probe not covalently linked to the protein is found in the aqueous layer. The denatured protein itself resides at the interface of the two layers. With this method, it was established that no detectable labeling of the lipids had occurred and, provided the probe was used when freshly made, only small amounts (about 5–10%) were noncovalently associated with the protein.

The labeled sarcoplasmic reticulum was also subjected to $NaDodSO_4$ gel electrophoresis (C. J. Restall, D. A. Elliot, and W. V. Weber, unpublished results), which also indicated that the probe was predominantly associated with the ($Ca^{2+}$–$Mg^{2+}$)ATPase, the results being qualitatively similar to those described by Burkli & Cherry (1981).

*Polarized Decay Data.* Four independent samples of the purified sarcoplasmic reticulum were taken and labeled as described. For each sample, collection of polarized data in an alternating sequence of four (HV, HH) and three (VV, VH) data sets was carried out. After reduction and inspection of the data following conversion to $S(t)$ and $R(t)$, it was evident (Figure 2) that (i) three of the data sets gave rise to $S(t)$ curves, which were identical by simple visual inspection, (ii) $S(t)$ for the odd data set obviously decayed much faster than those for the others, probably due to some leakage of air into the cuvette during the experiment or incomplete flushing with nitrogen before the experiment, (iii) $R(t)$ values for the three were not as superimposable as the corresponding $S(t)$ values but the agreement between smoothed curves was good to about 0.002 throughout the 5–510-μs time span of the data, (iv) $R(t)$ for the odd curve, while very similar in form to the others, was fairly uniformly lower by about 0.005, (v) all the $S(t)$ values were obviously nonexponential by the visual inspection of

Table I: Nonlinear Least-Squares Vector Analysis of Combined Data Set for Multiexponential $s(t)$ and $r(t)$ without Further Specification of Models for Their Decay Except for Decay of $r(t)$ to a Constant Value[a]

| model[b] | $a_i/\sum\alpha_i$ | $\tau$ ($\mu$s) | $\beta$ | $\phi$ ($\mu$s) | $\chi^2$ | $\chi^2_\nu$[c] |
|---|---|---|---|---|---|---|
| (a) 3$s$, (2 + $C$)$r$ | 0.155 ± 0.004 | 5.6 ± 0.2 | 0.021 ± 0.001 | 19.0 ± 1.5 | $1.410 \times 10^5$ | 14119 |
| | 0.147 ± 0.001 | 71 ± 1 | 0.018 ± 0.001 | 152 ± 16 | | |
| | 0.698 ± 0.002 | 306 ± 0.5 | 0.026 ± 0.001 | ∞ | | |
| | | | $r_0$ = 0.065 ± 0.001 | | | |
| (b) 4$s$, (2 + $C$)$r$ | 0.241 ± 0.016 | 2.9 ± 0.1 | | | | |
| | 0.065 ± 0.002 | 27.3 ± 1.3 | 0.020 ± 0.001 | 11.8 ± 0.9 | $8.20 \times 10^6$ | 8229 |
| | 0.179 ± 0.014 | 136 ± 8 | 0.021 ± 0.001 | 107 ± 5 | | |
| | 0.515 ± 0.017 | 333 ± 5 | 0.027 ± 0.001 | ∞ | | |
| | | | $r_0$ = 0.068 ± 0.001 | | | |
| (c) 4$s$, (3 + $C$)$r$ | 0.218 ± 0.014 | 3.1 ± 0.2 | 0.049 ± 0.022 | 2.6 ± 0.6 | $7.81 \times 10^6$ | 7846 |
| | 0.064 ± 0.002 | 26.2 ± 1.3 | 0.016 ± 0.001 | 27 ± 4 | | |
| | 0.177 ± 0.012 | 130 ± 7 | 0.017 ± 0.001 | 154 ± 20 | | |
| | 0.542 ± 0.014 | 331 ± 4 | 0.026 ± 0.001 | ∞ | | |
| | | | $r_0$ = 0.108 ± 0.022 | | | |

[a] The error estimates given, being obtained from the variance–covariance matrix are appropriate *only* when the fit between the calculated and data curves is statistically adequate. The apparent high accuracy of some of the parameters of inadequate fits should not be taken as an indication of goodness of fit. [b] See text for explanation of the notation. [c] $\chi^2_\nu$ is calculated as $\chi^2/\nu$ with the number of degrees of freedom $\nu = 2N - n - m$ being obtained from the number of points $N$ per curve, the number $n$ of independent parameters of $s(\alpha, \tau)$ and $m$, those for $r(\beta, \phi)$, where $N = 505$ and $n$ and $m$ are 6 and 5 for model a, 8 and 5 for model b, and 8 and 7 for model c. From these values, according to the criteria given in the text and from, for example, Figures 3–5 comparing the fits of model a–c, only model c is complex enough to simulate the data adequately; e.g., the change in $\chi^2$ between the (2 + $C$)$r$ and (3 + $C$)$r$ models for the two degrees of freedom gained is given by $[8229 \times (2 \times 505 - 8 - 5) - 7846 \times (2 \times 505 - 8 - 7)]/8229 = 48.3$, i.e., $>20\chi^2_\nu$ per degree of freedom.

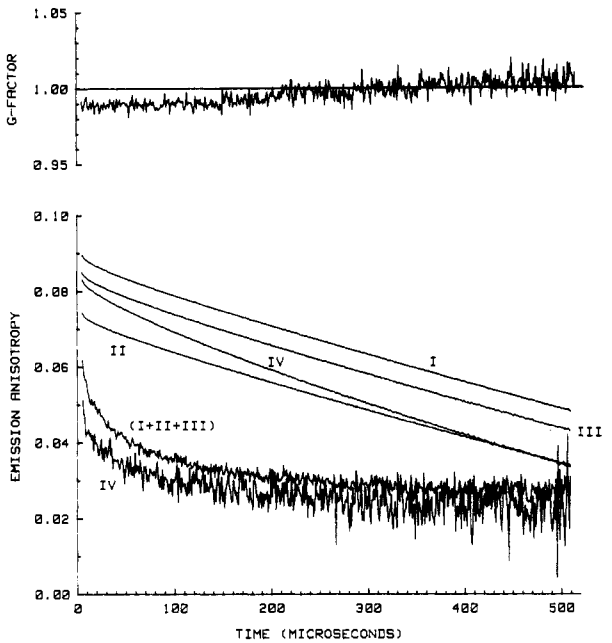


FIGURE 2: Summary of polarized decay data examined. The upper curves I–IV in the main part of the figure are the separate $S(t)$ functions (eq 19) on a semilogarithmic scale of 2 decades (2.8–4.8), including the "odd" data set (IV). The lower, noisy curves are the emission anisotropy decay functions $R(t)$ (eq 18) for the "odd" (IV) and combined (I + II + III) data sets. The upper panel illustrates the nonideality of the time dependence of the $G$ factors $[G(t) = I_{HH}(t)/I_{HV}(t)]$ used to normalize the polarized intensities $I_{VV}(t)$ appearing in the total emission intensity and emission anisotropy expressions.

semilogarithmic plots and evidently would require at least three exponential components to describe them adequately, and (vi) all the $R(t)$ values were also, as expected, nonexponential and in line with previous data (Moore et al., 1979; Restall et al., 1981; Burkli & Cherry, 1981; Speirs et al., 1983) visually exhibited an initial fast decay followed by a much slower one that tapered into an essentially constant non-zero value within the 0.5-ms time span of the experiment.

In view of these observations and the relatively high apparent noise level in $R(t)$, the three strictly comparable VV and VH data sets were combined to obtain a more accurate data set from which the parameters determining $R(t)$ might be more realistically and accurately obtained. These data, as $S(t)$ and $R(t)$, are displayed in Figure 3 together with the odd data set for comparison.

*Initial Analysis.* The five data sets, four original and one combined, were analyzed separately. Initial analyses were for (a) a triple-exponential decay of $s(t)$ combined with an anisotropy decay $r(t)$ described by two exponentials and a constant, designated 3$s$, (2 + $C$)$r$, (b) 4$s$, (2 + $C$)$r$, and (c) 4$s$, (3 + $C$)$r$. Reasonable starting values for analysis a were obtained from the semilogarithmic presentations of $S(t)$ and $R(t)$, those for (b) and (c) each being derived by interpolation from the previous parameter values obtained. Similar progressions in fitting were obtained in each case, and the results for the combined data set are presented in Table I. Analyses for 5$s$, (3 + $C$)$r$ and 5$s$, (4 + $C$)$r$ were also carried through. Although there appeared to be some small further progression in the goodness of fit for the former over the 4$s$, (3 + $C$)$r$ case, the anisotropy parameters were virtually unchanged. Effectively, the only change in the excited-state decay parameters was that the short lifetime split into a slightly longer and considerably shorter pair, the latter having a lifetime of about 0.9 ± 0.4 $\mu$s, below the resolution of these experiments. On increasing the complexity to 5$s$, (4 + $C$)$r$, no further progression in fitting was observed. The intermediate of the three anisotropy decay components of the previous analysis merely split into two components whose partial anisotropies and correlation times (the latter only about a factor of 2 different) were extremely ill defined (coefficients of variation about 3–5). Further analyses invoking specific models were therefore carried out on the basis of a four-exponential $s(t)$.

In all the comparisons for progression of goodness of fit, the criteria were taken to be (i) visual improvement in randomness of the residuals, e.g., $L_{VV} = (I_{VV} - i_{VV})$ (and of their autocorrelation functions),[3] between calculated and experimental

[3] The autocorrelation function $A(T)$ of residuals $L(t)$ is defined on an infinite data set as $A(T) = [\int L(t)L(t + T)\,dt]/A(0)$. Since the data set is finite, the autocorrelation functions calculated and presented here are defined on repeating sequences of $N$ residuals. Such a function is mirror symmetric about $T = N/2$ ($N$ is even) or $T = (N/2) + 1$ ($N$ is odd) in the first of its repeating cycles and is therefore not displayed beyond this symmetry point. Note that, for comparison purposes, the time origin for the autocorrelation functions presented has been shifted from 0 to 5 $\mu$s to enable easier identification of changes in the short-time correlations for different analyses.

curves and (ii) a change in the unweighted $\chi^2$

$$\chi^2 = \sum_{k=1}^{N} L_{Vk}^2 + L_{Hk}^2 \quad (24)$$

for the two orthogonally polarized components taken together over the $2N$ data points in each data set of about 10 or more reduced $\chi^2$ ($\chi_\nu^2$) per additional variable parameter. The reduced $\chi^2$ is calculated as the $\chi^2$ per degree of freedom: $\chi_\nu^2 = \chi^2/\nu$, where $\nu = 2N - n - m$, $n$ being the number of $s(t)$ parameters ($\alpha$, $\kappa = 1/\tau$) fitted and $m$ the number of $r(t)$ parameters ($\beta$, $\gamma = 1/\phi$) fitted. The same procedure is used for the $s(t)$ and $r(t)$ constructed from these components with their appropriately propagated residuals. As $s(t)$ is independent of $r(t)$ and, in the cases considered here where homogeneity of phosphorescence emission is assumed (see below), $r(t)$ is independent of $s(t)$, $\nu_s = N - n$ and $\nu_r = N - m$. These criteria are demonstrated in Figure 3, where data fits to $I_{VV}(t)$, $I_{VH}(t)$, $S(t)$, and $R(t)$ along with the residuals and autocorrelation functions are shown for the $3s$, $(2 + C)r$ analysis of the combined data set, and in Figures 4 and 5, in the latter of which the fits to $I_{VV}(t)$ and $I_{VH}(t)$ are represented only via the residuals and their autocorrelation functions, for the $4s$, $(2 + C)r$ and $4s$, $(3 + C)r$ analysis, respectively.

All the fits to the data were also examined with Poisson weighting of the residuals, e.g., $L_{VV} = (I_{VV} - i_{VV})/\sqrt{i_{VV}}$. Despite the absence of any good theoretical foundation for this weighting procedure for this kind of data, it did render the residuals for the orthogonally polarized components of the emission and also, appropriately propagated, those for the total emission and emission anisotropy somewhat more uniform over the relatively small range of intensity covered in these experiments. However, it did not alter any of the inferences about the relative merits of the fits of the theoretical models to the data made above according to the criteria laid out there.

*Modeled Analyses.* By use of the results of the $4s$, $(3 + C)r$ analyses as reasonable starting values, all five data sets were analyzed for an anisotropy decay model corresponding to a monoexponential approximation to segmental reorientational relaxation about some unique axis ($m$) in the macromolecular frame, all or part of the macromolecular population being free to rotate about the bilayer normal:

$$r(t) = \beta \exp(-t/\phi) + \beta_{m1} \exp(-4D_m t) + \beta_{m2} \exp(-D_m t) + \beta_{m3} \quad (25)$$

The results of this analysis for the combined data set, designated $4s$, $(1 + \text{ARB SEG} + C)r$ to indicate arbitrary orientation with respect to the bilayer normal of the axis about which the segmental motion occurs, are given in Table II and visualized in Figure 6. To emphasize the reality of the segmental motion, these may be compared with the results of a $4s$, $(\text{ARB SEG} + C)r$ analysis on these data displayed in Figure 7. In the absence of an immobilized fraction of the macromolecular population, the first term, $\beta \exp(-t/\phi)$, corresponds approximately to (i) $0.4\sum_j B_{pj} \exp(-t/\phi_{pj})$, (ii) $0.4P_2(\cos\theta_a)P_2(\cos\theta_e)\langle P_2(\cos\theta_p)\rangle^2\sum_{j'} B_{sj'} \exp(-t/\phi_{sj'})$, or (iii) $0.4\{\sum_j B_{pj} \exp(-t/\phi_{pj})[\sum_{j'} B_{sj'} \exp(-t/\phi_{sj'}) + \langle P_2(\cos\theta_s)\rangle^2] + P_2(\cos\theta_a)P_2(\cos\theta_e)\langle P_2(\cos\theta_p)\rangle^2\sum_{j'} B_{sj'} \exp(-t/\phi_{sj'})\}$ in eq 17, provided that $\phi_{pj}$ and $\phi_{sj'} \ll (4D_m)^{-1}$, depending on whether (i) the axis $\vec{p}$ of the segment having the phosphor bound rigidly to it reorients directly about the macromolecular axis $\vec{m}$, (ii) the phosphor-bearing segment reorients on a faster (submicrosecond) timescale than the data can resolve about a segmental axis $\vec{s}$ that reorients about $\vec{m}$ on the slower timescale indicated, or (iii) both axes $\vec{p}$ and $\vec{s}$ reorient on this slower timescale. The apparent partial anisotropy $\beta$ is obviously a complicated weighted average value but may correspond roughly with $0.4[P_2(\cos\theta_{ae}) - P_2(\cos\theta_a)P_2(\cos\theta_e)]\langle P_2(\cos\theta_p)\rangle^2$ in case i, with $0.4P_2(\cos\theta_a)P_2(\cos\theta_e)\langle P_2(\cos\theta_p)\rangle^2[1 - \langle P_2(\cos\theta_s)\rangle^2]$ in case ii, and with $0.4[P_2(\cos\theta_{ae}) - P_2(\cos\theta_a)P_2(\cos\theta_e)]\langle P_2(\cos\theta_p)\rangle^2[1 - \langle P_2(\cos\theta_s)\rangle^2]$ in case iii. The phosphorescence polarization of erythrosinyl isothiocyanate in a rigid medium has been reported to be $p_f = 0.25$ (Garland & Moore, 1979), corresponding to a fundamental zero point anisotropy $r_f = 2p_f/(3 - p_f) = 0.4P_2(\cos\theta_{ae}) = 0.18$. However, the value obtained for $r_0$, the zero point anisotropy on the microsecond timescale, in the $4s$, $(3 + C)r$ analysis is on the order of 0.11 (see Table I). Therefore, it seems likely that the appropriate choice is case ii or, alternatively, a model corresponding to some arbitrary number of rapidly (submicrosecond) reorienting segments between the phosphor and the segment reorienting on the microsecond timescale. This is borne out by the results of the analyses according to eq 25 presented in Table II for which all but data set IV give $r_0$ values close to 0.08. Within the criteria for progression in fitting indicated above, the fits of the data to this model are identical with those for the $4s$, $(3 + C)r$ case. The high value of $\beta$ and short correlation time $\phi$ obtained for data set IV, also seen in $\beta_1$ and $\phi_1$ in the $4s$, $(3 + C)r$ analysis of that data set, appear to result from chance correlations in the first few microseconds of data registered. This is not assigned any significance in comparison with the other data sets, particularly since, as seen in Table II, the $\beta_m$ and $D_m$ correspond quite well with those for the other data sets. The means and standard errors of these parameters on the basis of the values obtained for the three separate data sets that were combined are

$$\beta_{m1} = 0.013 \pm 0.002 \qquad \beta_{m2} = 0.016 \pm 0.001$$
$$D_m^{-1} = 145 \pm 15\ \mu s \qquad \beta_{m3} = 0.026 \pm 0.001$$

As can be seen by comparison with Table II, data set $C$, the means correspond rather well with those obtained from the analysis of the combined data sets, while the standard errors show the expected improvement. The level of error committed in estimating $\beta_m$ and $D_m$ values via a model excluding the segmental motion is indicated by the results of the $4s$, $(\text{ARB SEG} + C)r$ analysis for the combined data set

$$\beta_{m1} = 0.016 \qquad \beta_{m2} = 0.017 \qquad D_m^{-1} = 100\ \mu s$$
$$\beta_{m3} = 0.028$$

the poor fit of which to the data is visualized in Figure 7. The standard error estimates are not given since the lack of a statistically adequate fit for this model to the data invalidates the variance/covariance estimates obtained. It can also be seen from Table II, data set C, that, despite strictly incorrect weighting, a direct analysis of the $R(t)$ decay curve itself gave essentially the same results as were obtained in the full vector analysis of the combined data set for the model represented in eq 25. Such a direct analysis, even with proper weighting, is valid only if the emitting and rotating species are homogeneous or if either, but not both, are heterogeneous.

Attempts were also made to analyze the data with an anisotropy decay corresponding to eq 25 with the first term replaced by $\beta_1 \exp(-t/\phi_1) + \beta_2 \exp(-t/\phi_2)$ as a better approximation to the fast phase of segmental reorientation. Sensible results were not obtained with any of the four original data sets, presumably because of noise limitations on the accuracy of the data. A result was, however, obtained for the combined data set and is also presented in Table II. The improvement in overall $\chi^2$ did not appear to be significant, nor did that for $r(t)$, both amounting to about $7\chi_\nu^2$ per degree of freedom lost. Moreover, the values of $r_0$, $\beta_m$, and $D_m$ did not

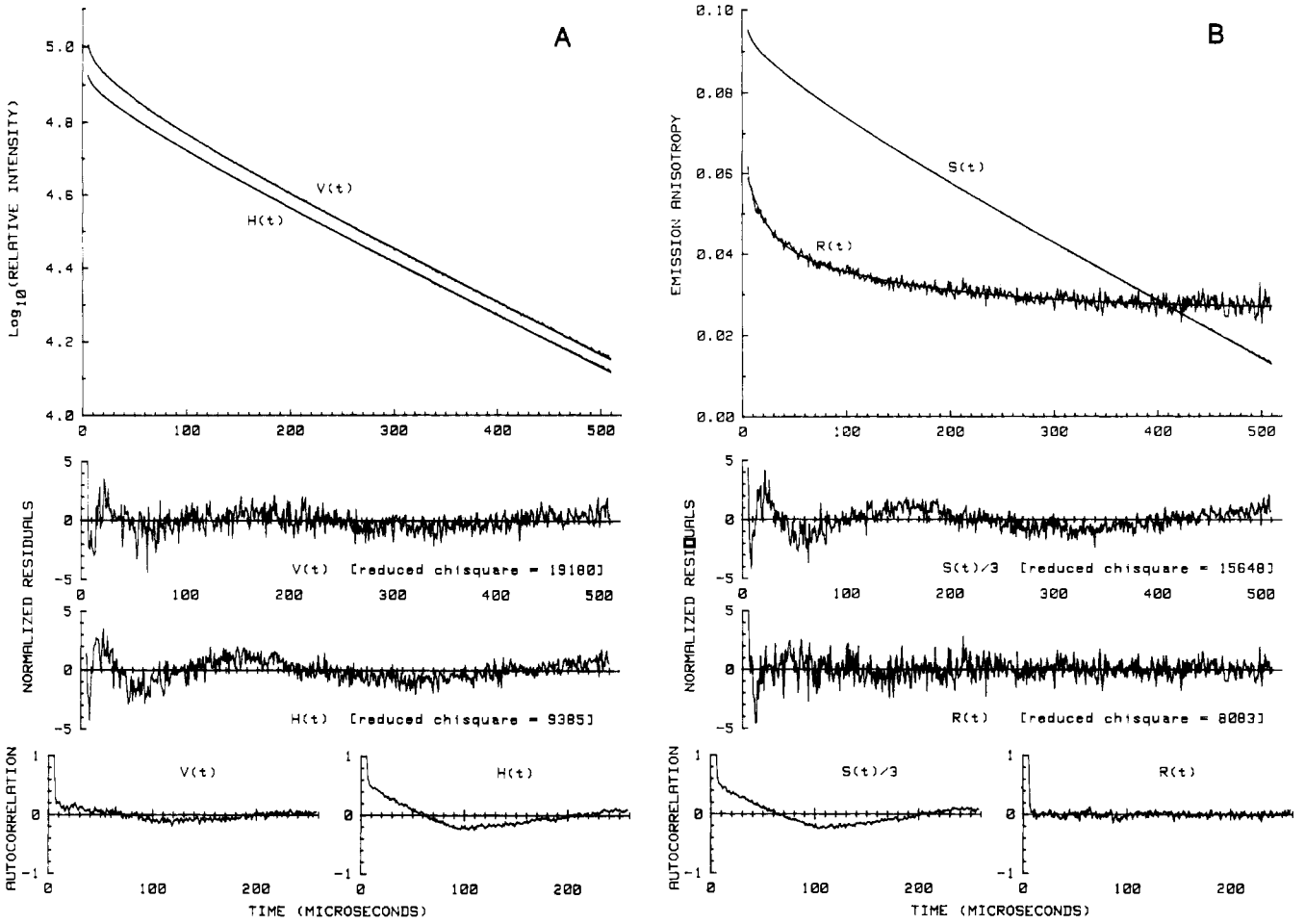


FIGURE 3: Comparison of data from the combined data set with theoretical curves generated from the parameters, summarized in Table I, of the best nonlinear least-squares fit of the model $3s$, $(2 + C)r$. (A) (Upper) Semilogarithmic comparisons of experimental and theoretical orthogonally polarized decay curves $I_{VV}(t)$ with $i_{VV}(t)$ [$V(t)$] and $I_{VH}(t)$ with $i_{VH}(t)$ [$H(t)$]; (lower) residuals and their autocorrelation functions for the above fits. (B) (Upper) Comparison of $S(t)/3$ with $s(t)/3$ on a semilogarithmic scale of 1 decade (4.0–5.0) and of $R(t)$ with $r(t)$ on a linear scale; (lower) residuals and their autocorrelation functions for these fits.

Table II: Results of Nonlinear Least-Squares Vector Analysis of All Data Sets with $s(t) = \sum_{i=1}^{4} \alpha_i \exp(-t/\tau_i)$ and $r(t) = \beta \exp(-t/\phi) + \beta_{m1} \exp(-4D_m t) + \beta_{m2} \exp(-D_m t) + \beta_{m3}$

| data set | $\beta$ | $\phi$ ($\mu$s) | $\beta_{m1}$ | $\beta_{m2}$ | $D_m^{-1}$ ($\mu$s) | $\beta_{m3}$ | $r_0$ |
|---|---|---|---|---|---|---|---|
| I | 0.022 ± 0.004 | 5.7 ± 1.4 | 0.017 ± 0.004 | 0.015 ± 0.005 | 160 ± 60 | 0.026 ± 0.001 | 0.079 ± 0.005 |
| II | 0.031 ± 0.008 | 4.2 ± 0.8 | 0.010 ± 0.004 | 0.016 ± 0.003 | 135 ± 35 | 0.026 ± 0.001 | 0.083 ± 0.008 |
| III | 0.023 ± 0.008 | 4.6 ± 1.3 | 0.011 ± 0.005 | 0.016 ± 0.004 | 130 ± 45 | 0.029 ± 0.001 | 0.080 ± 0.009 |
| IV[a] | 0.20 ± 0.21 | 1.7 ± 0.6 | 0.010 ± 0.007 | 0.012 ± 0.007 | 140 ± 90 | 0.023 ± 0.001 | 0.25 ± 0.21 |
| C[b] | 0.024 ± 0.003 | 4.9 ± 0.7 | 0.014 ± 0.003 | 0.015 ± 0.003 | 150 ± 40 | 0.027 ± 0.001 | 0.080 ± 0.004 |
| | (0.019 ± 0.003) | (6.9 ± 1.2) | (0.013 ± 0.002) | (0.015 ± 0.002) | (170 ± 35) | (0.026 ± 0.001) | (0.073 ± 0.004) |
| C[c] | 0.074 ± 0.057 | 2.0 ± 0.7 | 0.012 ± 0.005 | 0.013 ± 0.006 | 200 ± 125 | 0.026 ± 0.002 | 0.135 ± 0.060 |
| | 0.010 ± 0.004 | 16 ± 5 | | | | | |

[a] Data set IV is the odd set for which $s(t)$ differs substantially from those of data sets I–III as discussed in the text. [b] Combined data set C made up of I + II + III; results for *direct* unweighted EA decay analysis in parentheses. [c] Analysis of combined data set I + II + III replacing the approximation of $\beta \exp(-t/\phi)$ by $\beta_1 \exp(-t/\phi_1) + \beta_2 \exp(-t/\phi_2)$. With the criteria given in the text, no significant improvement in $\chi^2$ is seen between these two models: $\chi^2(1) = 7.91 \times 10^6$ and $\chi^2_\nu(1) = 7939$ compared with $\chi^2(2) = 7.80 \times 10^6$ and $\chi^2_\nu(2) = 7848$ for two fewer degrees of freedom, a change in total $\chi^2$ of only about $7\chi^2_\nu$ per degree of freedom.

change within their, now considerably larger, standard error estimates.

*Interpretation of* $\beta_m$. According to eq 6, 7, and 17, the $\beta_m$ values represent the fundamental values $B_m$ scaled by the factor $P_2(\cos\theta_a)P_2(\cos\theta_e)\langle P_2(\cos\theta_p)\rangle^2$ (case i) or its product with $\langle P_2(\cos\theta_s)\rangle^2$ (cases ii and iii). Thus, the quotient $Q$ of the first two $\beta_m$ terms is given by

$$Q = \beta_{m1}/\beta_{m2} = B_{m1}/B_{m2} = (\tan^2\theta_m)/4 \qquad (26)$$

from which the angle $\theta_m$ made by the macromolecular axis $\vec{m}$ about which segmental reorientation occurs and the bilayer normal $\vec{n}$ can be calculated as

$$\theta_m = \arctan(2Q^{1/2}) \pm [(1 + 4Q)Q^{1/2}]\sigma(Q) \qquad (27)$$

the value of the standard error $\sigma(Q)$ being obtained from the $\beta_{m1}$ and $\beta_{m2}$ variance and covariance estimates. The values of $B_{m1}$, $B_{m2}$, and $B_{m3}$ are presented as a function of $\theta_m$ in Figure 8, along with the critical ratio $Q = B_{m1}/B_{m2}$ in the range of $\theta_m$ of concern here. The constant term in the depolarization factor for rotation of the macromolecule about the bilayer normal is given by

$$B_{m3} = P_2^2(\cos\theta_m) = \left(\frac{3}{2}\frac{\beta_{m2}}{4\beta_{m1} + \beta_{m2}} - \frac{1}{2}\right)^2 \qquad (28)$$

On scaling this, a value $\beta'_{m3}$ corresponding to the measured $\beta_{m3}$ within the propagated error will be found if the macro-

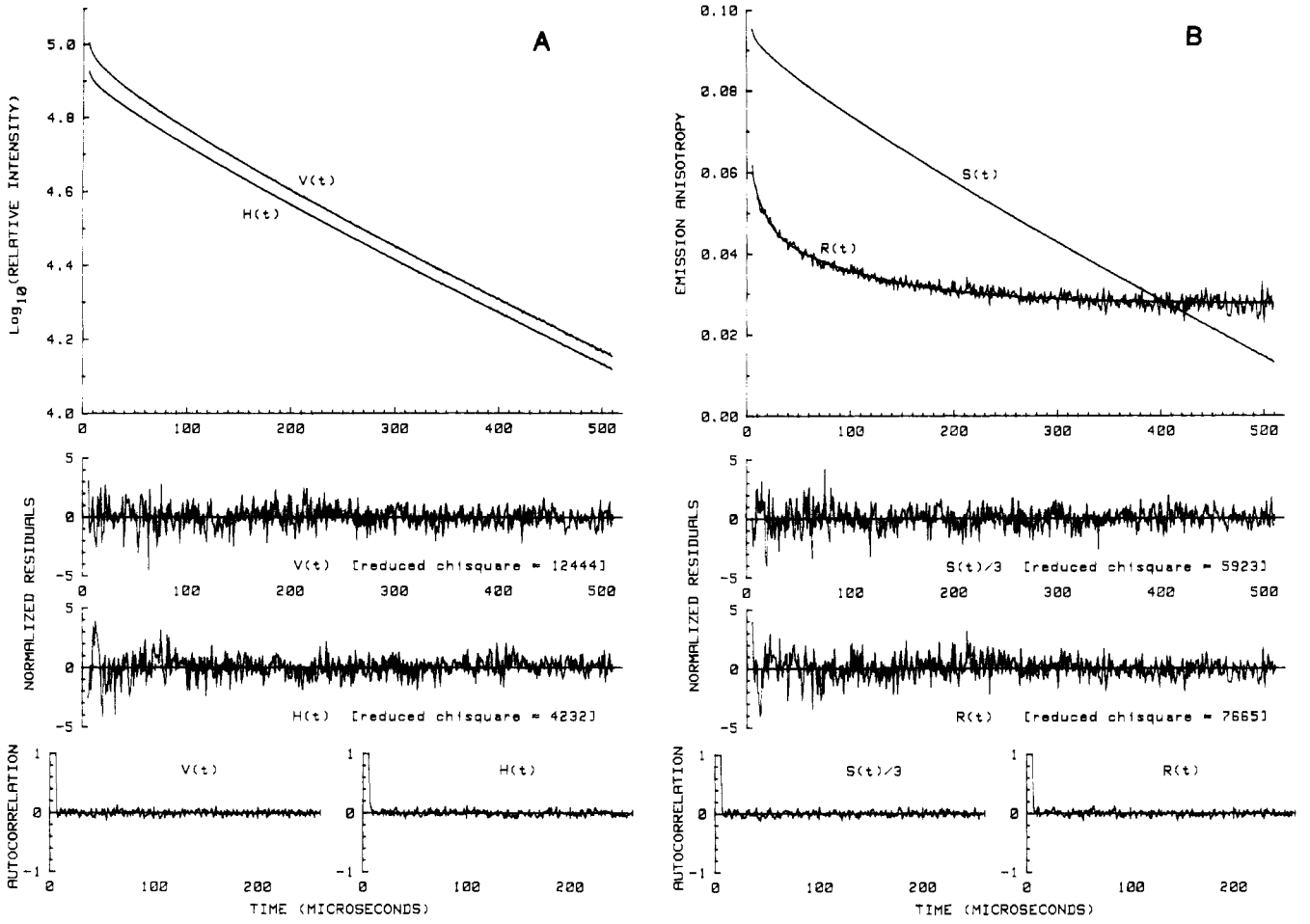


FIGURE 4: Comparison of data from combined data set with theoretical curves generated from the parameters, summarized in Table I, of the best nonlinear least-squares fit of the model $4s$, $(2 + C)r$. (A) (Upper) Semilogarithmic comparison for experimental and theoretical orthogonally polarized decay curves $I_{VV}(t)$ with $i_{VV}(t)$ $[V(t)]$ and $I_{VH}(t)$ with $i_{VH}(t)$ $[H(t)]$; (lower) residuals and their autocorrelation functions. (B) (Upper) Comparison of $S(t)/3$ with $s(t)/3$ on a semilogarithmic scale of 1 decade (4.0–5.0) and of $R(t)$ with $r(t)$ on a linear scale; (lower) residuals and their autocorrelation functions for these fits.

Table III: Results of Interpretation of Data Analyses in Terms of Mean Orientation $\theta_m$ of the Rapidly Reorienting Segment with Respect to Bilayer Normal, Limiting Anisotropy $\beta'_{m3}$ Expected from It, and Maximum and Minimum Fractions of Immobile Protein That Could Account for the Discrepancy $\beta''_{m3}$ between This and the Value $r_\infty = \beta_{m3} = \beta'_{m3} + \beta''_{m3}$ Obtained in the Analysis

| data set | $\beta_{m1}/\beta_{m2}$ | $\theta_m$ (deg) | $\beta'_{m3}$ | $\beta''_{m3}$ | $f_{min}$[a] | $f_{max}$ |
|---|---|---|---|---|---|---|
| I | 1.15 ± 0.65 | 65 ± 6 | 0.002 ± 0.001 | 0.024 ± 0.001 | 0.13 ± 0.01 | 0.42 ± 0.04 |
| II | 0.62 ± 0.34 | 58 ± 7 | <0.001 | 0.025 ± 0.001 | 0.14 ± 0.01 | 0.49 ± 0.04 |
| III | 0.67 ± 0.46 | 59 ± 9 | <0.001 | 0.029 ± 0.001 | 0.16 ± 0.01 | 0.52 ± 0.05 |
| IV | 0.82 ± 1.00 | 61 ± 15 | 0.001 ± 0.001 | 0.023 ± 0.002 | 0.13 ± 0.01 | 0.50 ± 0.09 |
| C[b] | 0.93 ± 0.40 | 63 ± 5 | 0.001 ± 0.001 | 0.026 ± 0.001 | 0.14 ± 0.01 | 0.47 ± 0.03 |
| C[c] | 0.87 ± 0.72 | 62 ± 10 | 0.001 ± 0.001 | 0.025 ± 0.002 | 0.14 ± 0.01 | 0.49 ± 0.06 |

[a] $f_{min}$ calculated by assuming $r_f = 0.18$ (Garland & Moore, 1979) with a standard error arbitrarily taken as 0.01. [b] See footnote *b* in Table II. [c] See footnote *c* in Table II.

molecular population is homogeneous with respect to its rotation about the membrane bilayer normal. From the results of the above analysis of $\beta_m$ presented in Table III, it is obvious that this is not so and that, therefore, some fraction of the protein is either stationary or rotating too slowly to be resolved in the time span (0.5 ms) of the data.

Several possibilities exist for the estimate of this stationary fraction having an anisotropy $\beta''_{m3}$ defined by

$$\beta''_{m3} = \beta_{m3} - \beta'_{m3} \tag{29}$$

Presumably, in all cases the stationary fraction represents aggregated molecular species. If all types, microsecond and submicrosecond, of the segmental motions in these species are unaffected by aggregation, then the immobilized fraction $f$ is simply given by $\beta''_{m3}/\sum_{i=1}^{3}\beta_{mi}$. At the other extreme, however, if all types of segmental motion are arrested in the aggregated forms, $f = \beta''_{m3}/r_f$, where $r_f$, the fundamental phosphorescence anisotropy, has the value 0.18 (Garland & Moore, 1979). In the intermediate case where the microsecond but not the submicrosecond segmental motion is arrested, $f = \beta''_{m3}/r_0$. More complex possibilities obviously exist, but the maximum range of immobilized fraction is given by the above two extreme cases, and the results obtained for the five data sets analyzed are also given, along with their propagated error estimates, in Table III.

A similar analysis for the immobile fraction has been described previously for the rotation of an oligomeric cytochrome P-450 in reconstituted phospholipid vesicles monitored by the delayed fluorescence anisotropy of a diiodofluorescein derivative that exhibits only the uniaxial rotation on the microsecond

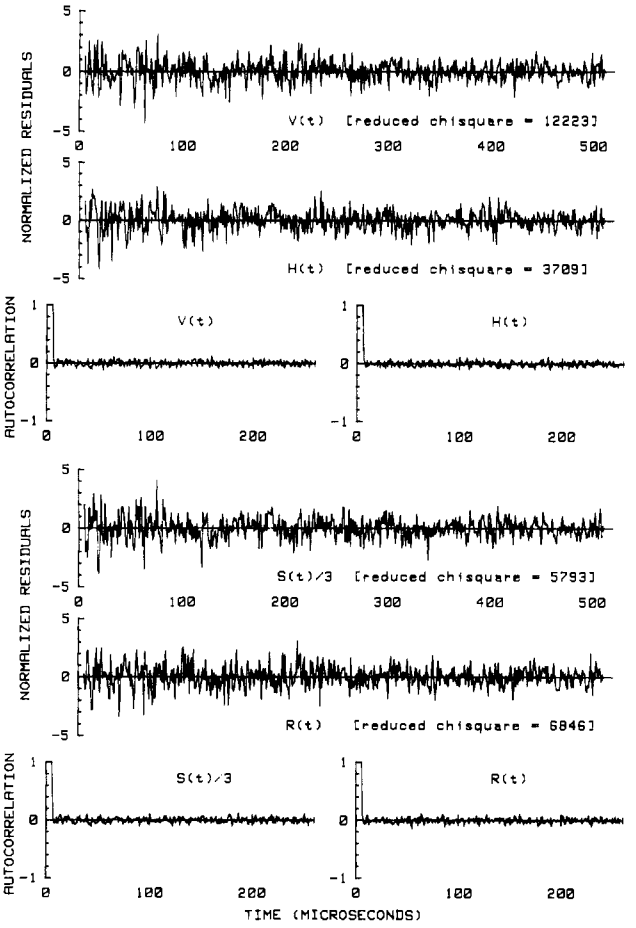


FIGURE 5: As in Figure 4 but for the model $4s$, $(3 + C)r$ (see Table I), depicting only residuals and their autocorrelation functions. No visual differences in the direct fits between these data and the data of Figure 4 are detectable on this scale.

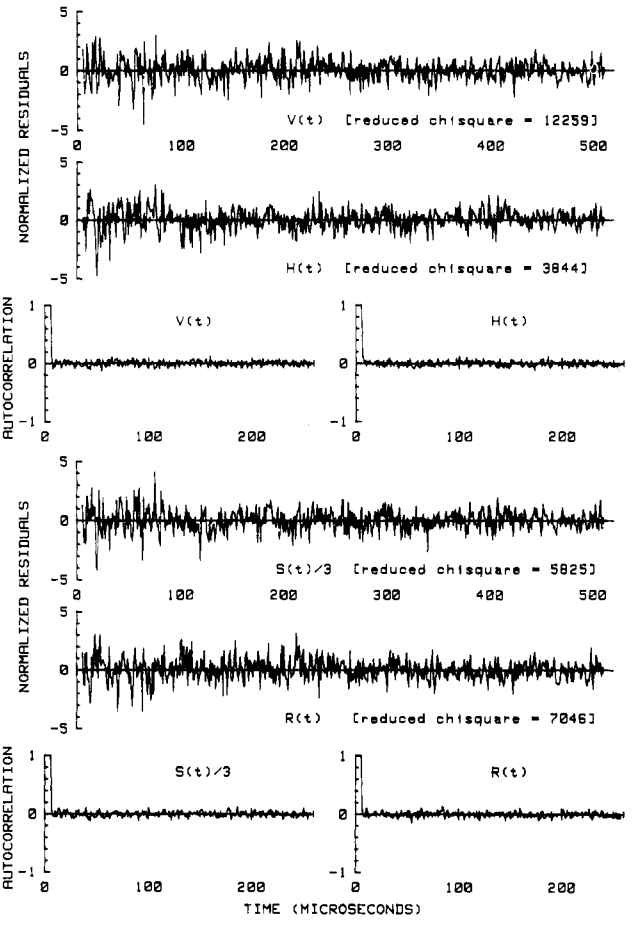


FIGURE 6: As in Figure 5 but for the model $4s$, $(1 + \text{ARB SEG} + C)r$ (see Table II and eq 25).

timescale (Greinert et al., 1982).

*Heterogeneity*. The results of the above analyses indicate a high degree of heterogeneity of the macromolecular population vis-à-vis its anisotropy decay behavior. The rotational diffusion coefficients $D_m$ obtained for the mobile fraction in these analyses correspond to a viscosity of about 20–25 P for the membrane, calculated by assuming that the effective rotating unit of the ATPase is a cylindrical protein segment of molecular weight 35 000 having a height ($h$) of 40–45 Å in the membrane from

$$D_m = kT/(4\pi a^2 h\eta) \qquad (30)$$

where $k$ is the Boltzmann constant, $a$ is the radius of the segment, and $\eta$ is the effective membrane viscosity, remembering that only about one-third of the protein of overall molecular weight 105 000 is buried in the bilayer, the rest experiencing relatively negligible viscous opposition to its rotation in the external aqueous glycerolic environment ($\eta \simeq$ 0.15 P). However, it is not entirely clear that the estimates of $D_m$ and $\beta_{m3}$ do not represent to some extent weighted averages for monomer and/or various aggregated species, the lower multimers affecting mainly $D_m$ and the higher ones $\beta_{m3}$. Other hydrodynamic or structural data would be required in order to resolve this question definitively, e.g., parallel determination of the lateral diffusion coefficient (Peters & Cherry, 1982).

The above analyses have been carried out on the assumption that the phosphorescence emission itself is homogeneous; i.e., each and every erythrosin label exhibits identical excited-state decay behavior, in particular whether or not it is bound to a monomeric or aggregated protein. However, a pointer to the probable essentially homogeneous nature of the emission is provided by sample IV in which the decay of the phosphorescence is noticeably more rapid. The anisotropy decay course nevertheless remains remarkably similar to those observed in the other cases (Figure 2). This constitutes good evidence for a lack of correlation between emission and emission anisotropy decays (T. M. Jovin, personal communication).

## Discussion

Earlier studies of the rotational diffusion of the ($Ca^{2+}$–$Mg^{2+}$)ATPase in sarcoplasmic reticulum have demonstrated the complex nature of its movement (Kirino et al., 1978; Hoffmann et al., 1979; Restall et al., 1981; Burkli & Cherry 1981; Speirs et al., 1983). This work has indicated that segmental movements within the protein occur in addition to rotational movement of the whole protein in the lipid bilayer matrix.

In this study we have applied well-established theories of molecular movement to this biologically important system in order to produce a minimal description of its rotational diffusion. Previously, such a detailed analysis has only been performed on the much simpler system comprising bacteriorhodopsin reconstituted into dimyristoylphosphatidylcholine vesicles (Cherry & Godfrey 1981).

The simplest model consistent with the data is one that envisages the phosphor, or a segment to which it is rigidly bound, undergoing restricted rotational diffusion at rates too fast to be resolved on the time scale of the phosphorescence anisotropy decay experiment. The axis about which this

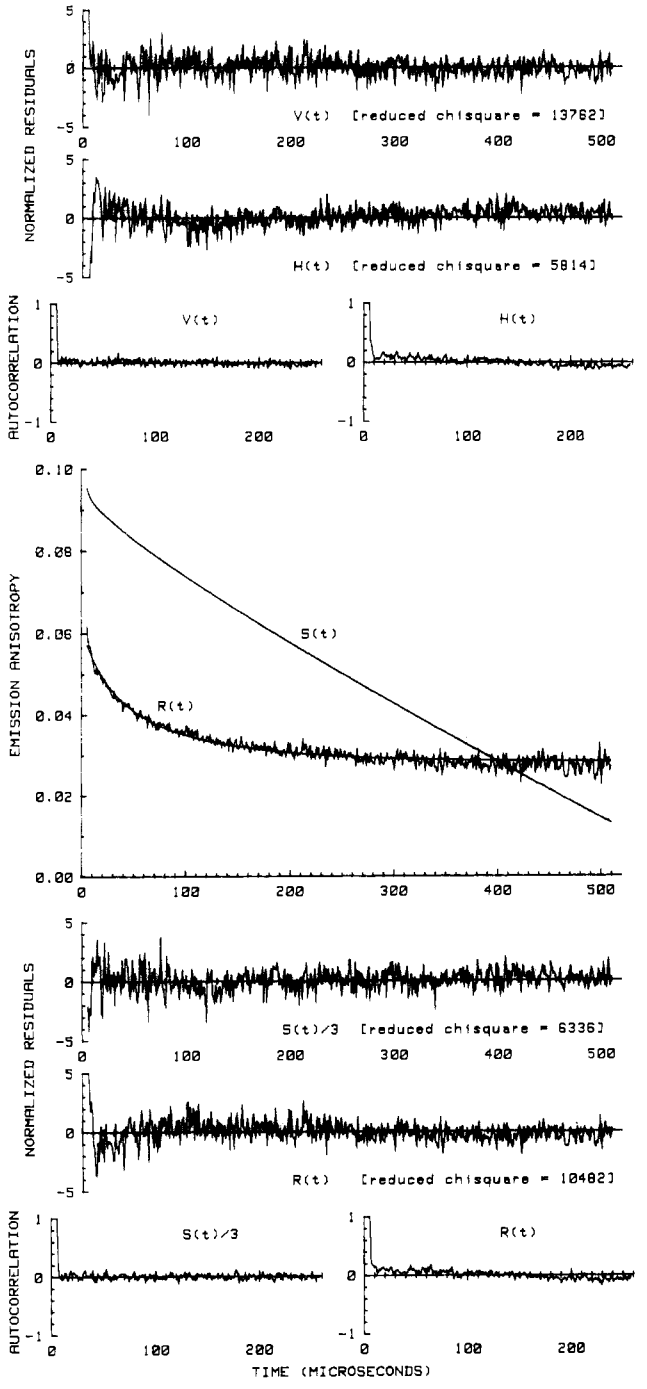


FIGURE 7: Comparison of data from the combined data set with theoretical curves generated from the parameters of the best nonlinear least-squares fit of the poor model 4*s*, (ARB SEG + *C*)*r*—compare eq 25 in text. (Upper) Residuals between experimental and theoretical orthogonally polarized decay curves $I_{VV}(t)$ with $i_{VV}(t)$ $[V(t)]$ and $I_{VH}(t)$ with $i_{VH}(t)$ $[H(t)]$ and their autocorrelation functions; (middle) comparison of $S(t)/3$ with $s(t)/3$ on a semilogarithmic scale of 1 decade (4.0–5.0) and of $R(t)$ with $r(t)$ on a linear scale; (lower) residuals and their autocorrelation functions for the $S(t)$ and $R(t)$ fits. No visual differences in the direct fits for $V(t)$ and $H(t)$, omitted here, between these data and the data of Figure 4 are detectable on that scale.

motion occurs is fixed in a segment that itself undergoes restricted rotational diffusion. This gives rise to the fastest component observable in the anisotropy decay (correlation time on the order of a few microseconds). The axis about which this rotation proceeds is fixed in the protein that rotates as a whole about the normal to the lipid bilayer, the rotational correlation times being on the order of 100 $\mu$s. Some fraction of the phosphor, however, is bound to protein that does not

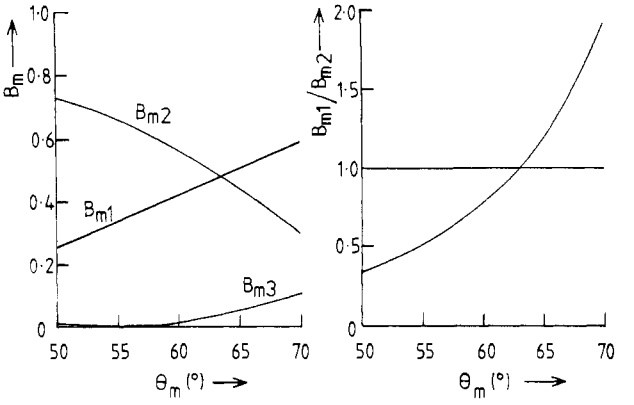


FIGURE 8: Variation of normalized partial anisotropies $B_{m1}$, $B_{m2}$, and $B_{m3}$ (eq 5 and 6) with the polar angle $\theta_m$ (left) and of the ratio $B_{m1}/B_{m2}$ (right) over the range of $\theta_m$ relevant in the present case.

rotate in the membrane, presumably corresponding to aggregated forms. In these, the very fast and slower segmental motions may or may not take place. Depending on which of these motions is assumed to occur in the immobilized protein fraction, the quantitative estimate of this fraction varies.

The assumptions inherent in interpretation by this simplest model are as follows. (i) There is a unique site of attachment of the phosphor or, at least, the axes in the macromolecule about which the very fast and slower segmental rotations occur are unique. This is not unreasonable since it might be expected that there would be a preferred binding site for the probe, rather than a situation in which many, equally probable sites exist. Good evidence for a single binding site comes, however, from studies on the binding of the closely related probe fluoresceinyl isothiocyanate (Mitchinson et al. 1982) to the ($Ca^{2+}$–$Mg^{2+}$)ATPase. This work has shown that the fluoresceinyl isothiocyanate binding site is a single lysine residue located 10 residues from the N-terminus of tryptic fragment B. In view of the structural and chemical similarity between the fluoresceinyl isothiocyanate molecule and the erythrosinyl isothiocyanate used in the present studies, it seems highly likely that they would bind to the same residue. (ii) As a result of the segmental motions, the phosphor absorption and emission transition moments $\vec{\mu}_a$ and $\vec{\mu}_e$ are azimuthally randomly distributed about the axis $\vec{m}$ fixed in the macromolecule at an angle $\theta_m$ to the bilayer normal $\vec{n}$. The rather extensive depolarization on both the microsecond and submicrosecond time scales from the limiting $r_0$ value indicates strongly that this condition is essentially fulfilled. This assumption is central to the subsequent interpretation of the results of data analysis with respect to the presence of mobile and immobile (aggregated) forms of the protein. If it is relaxed, the $\beta_m$ terms are more complex, containing functions of the angles made by $\vec{\mu}_a$ and $\vec{\mu}_e$ with $\vec{n}$, which are not completely averaged out [cf. Speirs et al. (1983)]. (iii) The protein fraction that rotates in the membrane does so in an essentially one-dimensional fashion with no appreciable "wobble" of the protein as a whole about the bilayer normal on the time scale of the rotation. (iv) The protein is present either as freely rotating monomer or as immobile aggregates, no appreciable fraction being present as, e.g., dimers or small multimers. This point needs to be carefully considered since aggregation of the ($Ca^{2+}$–$Mg^{2+}$)-ATPase is known to occur, particularly in aged preparations of sarcoplasmic reticulum (Chyn & Martonosi, 1977). The presence of protein aggregates too large to rotate on the time scale of our measurements can be detected and even quantitated by the methods described here. However, small multimers such as dimers or trimers could affect the interpretation

of the results, since they might be expected to rotate with correlation times not too dissimilar from those of the monomer. It is possible to detect the presence of small covalent aggregates relatively easily by polyacrylamide gel electrophoresis, and provided measurements are performed on freshly made sarcoplasmic reticulum suspensions, the proportion of these aggregates is negligible. Unfortunately, this method will not detect the presence of noncovalent aggregates whose presence in the membrane cannot therefore be eliminated from consideration. The presence or absence of these species might be established by reconstituting the ATPase in model fluid membrane systems and monitoring its rotational diffusion as a function of its concentration. (v) The multiexponential nature of the decay of the phosphorescence itself, while it may reflect heterogeneity of the environment of the probe within or between individual proteins with respect to triplet-state deactivation processes, is not connected with any heterogeneity of either segmental or whole protein rotational relaxation.

The need for a complete, theoretically sound, description of protein rotational diffusion data is important if meaningful relationships between movement and function are to be drawn. The function of this protein appears to be at least partially impaired in rigid reconstituted membranes (Gomez-Fernandez et al., 1980). A conformational change in the protein induced by its changed environment may be the cause of this. On the other hand, the fast segmental motion may be intimately involved in the protein function and the effect of changing the membrane environment attributable to retardation of this motion. It is difficult to see why rotation of the protein as a whole should be important per se to the enzyme function. It seems more likely that it simply monitors membrane states appropriate or inappropriate to functional performance.

Attempts have been made to relate some parameter from rotational diffusion data to the ATPase activity of the protein. In particular, interest has centered on the break at about 15 °C observed in the Arrhenius plot of calcium-dependent ATPase activity. This phenomenon has been ascribed either to a lipid phase transition (Hidalgo et al., 1976) or to a conformational change in the protein (Dean & Tanford, 1979; Anzai et al., 1978) although the balance of evidence seems to favor the latter possibility. Previous studies of ($Ca^{2+}$–$Mg^{2+}$)ATPase movement have also been interpreted in terms of a conformational change in the protein structure. Kaizu et al. (1980) using the saturation-transfer EPR technique and Hoffmann and co-workers (1979) using laser-flash photolysis both interpreted their results in terms of a conformational change in the protein around 15 °C. More recently, Burkli & Cherry (1981), also using flash photolysis, have demonstrated that if the anisotropy measured 20 $\mu$s after the exciting flash ($r_{20}$) is plotted in an Arrhenius representation, a discontinuity is observed at about 13 °C. These workers were careful not to assign too much significance to this result since the value of $r_{20}$ is determined by many factors. However, the result does suggest that some element of the ($Ca^{2+}$–$Mg^{2+}$)-ATPase movement is related to its function. By using the sort of data analysis described in this paper, we anticipate that it may be possible to accurately relate protein movements to function and possibly provide insights as to how a protein such as the ($Ca^{2+}$–$Mg^{2+}$)ATPase pumps calcium ions across the membrane.

Acknowledgments

We thank Elisa Morgan for valuable technical assistance during the course of this work, Dr. W. V. Weber for useful discussions and assistance with some earlier experiments, and Dr. C. L. Greenstock for drawing our attention to the work of Greinert et al. (1982) during preparation of the manuscript.

**Registry No.** ATPase, 9000-83-3.

References

Anzai, K., Kirino, Y., & Shimizu, H. (1978) *J. Biochem. (Tokyo) 84*, 815–821.

Austin, R. H., Chan, S. S., & Jovin, T. M. (1979) *Proc. Natl. Acad. Sci. U.S.A. 76*, 5650–5654.

Burkli, A., & Cherry, R. J. (1981) *Biochemistry 20*, 138–145.

Chapman, D., & Restall, C. J. (1982) *Biochem. Soc. Symp. 46*, 139–154.

Chen, R. F., & Bowman, R. L. (1965) *Science (Washington, D.C.) 147*, 729–732.

Cherry, R. J. (1979) *Biochim. Biophys. Acta 559*, 289–327.

Cherry, R. J., & Godfrey, R. E. (1981) *Biophys. J. 36*, 235–257.

Cherry, R. J., Cogoli, A., Oppliger, M., Schneider, G., & Semenza, G. (1976) *Biochemistry 15*, 3653–3656.

Chyn, Y., & Martonosi, A. (1977) *Biochim. Biophys. Acta 468*, 114–126.

Dale, R. E., & Eisinger, J. (1975) in *Biochemical Fluorescence: Concepts* (Chen, R. F., & Edelhoch, H., Eds.) Vol. 1, Chapter 4, Appendix C2, pp 275–278, Marcel Dekker, New York.

Dean, W. L., & Tanford, C. (1978) *Biochemistry 17*, 1683–1690.

Fletcher, R. (1971) *Atomic Energy Research Establishment Report, No. AERE-R6799*, HMSO.

Garland, P. B., & Moore, C. H. (1979) *Biochem. J. 183*, 561–572.

Gilbert, C. W. (1983) *NATO Adv. Study Inst. Ser., Ser. A 69A*, 604–606.

Gomez-Fernandez, J.-C., Goni, F. M., Bach, D., Restall, C. J., & Chapman, D. (1980) *Biochim. Biophys. Acta 598*, 502–516.

Gottleib, Y. Ya., & Wahl, Ph. (1963) *J. Chim. Phys. 60*, 849–856.

Greinert, R., Finch, S. A. E., & Stier, A. (1982) *Biosci. Rep. 2*, 991–994.

Hidalgo, C., Ikemoto, N., & Gergely, J. (1976) *J. Biol. Chem. 251*, 4224–4273.

Hoffmann, W., Sarzala, M. G., & Chapman, D. (1979) *Proc. Natl. Acad. Sci. U.S.A. 76*, 3860–3864.

Hoffmann, W., Sarzala, M. G., Gomez-Fernandez, J.-C., Goni, F. M., Restall, C. J., Chapman, D., Heppeler, G., & Kreutz, W. (1980) *J. Mol. Biol. 141*, 119–132.

Kaizu, T., Kirino, Y., & Shimizu, H. (1980) *J. Biochem. (Tokyo) 88*, 1837–1843.

Kawato, S., & Kinosita, K., Jr. (1981) *Biophys. J. 36*, 277–296.

Kinosita, K., Jr., Kawato, S., & Ikegami, A. (1977) *Biophys. J. 20*, 289–305.

Kinosita, K., Jr., Ikegami, A., & Kawato, S. (1982) *Biophys. J. 37*, 461–464.

Kirino, Y., Ohkuma, T., & Shimizu, H. (1978) *J. Biochem. (Tokyo) 84*, 111–115.

Lipari, G., & Szabo, A. (1980) *Biophys. J. 30*, 489–506.

Malan, N., Sabbadini, R., Scales, D., & Inesi, G. (1975) *FEBS Lett. 60*, 122–125.

Mitchinson, C., Wilderspin, A. F., Trinnaman, B. J., & Green, N. M. (1982) *FEBS Lett. 146*, 87–92.

Moore, C., Boxer, D., & Garland, P. (1979) *FEBS Lett. 108*, 161–166.

Peters, R., & Cherry, R. J. (1982) *Proc. Natl. Acad. Sci. U.S.A. 79*, 4317–4321.

Restall, C. J., Arrondo, J. L. R., Elliot, D. A., Jaskowska, A., Weber, W. V., & Chapman, D. (1981) *Biochim. Biophys. Acta 670*, 433–440.
Saffmann, P. G., & Delbruck, M. (1975) *Proc. Natl. Acad. Sci. U.S.A. 72*, 3111–3113.
Sarzala, M. G., & Michalak, M. (1978) *Biochim. Biophys. Acta 513*, 221–235.
Speirs, A., Moore, C. H., Boxer, D. H., & Garland, P. B. (1983) *Biochem. J. 213*, 67–74.
Steinberg, I. Z. (1975) in *Biochemical Fluorescence: Concepts* (Chen, R. F., & Edelhoch, H., Eds.) Vol. 1, Chapter 3, pp 79–113, Marcel Dekker, New York.
Steiner, R. F., & McAlister, A. (1957) *J. Polym. Sci. 24*, 105–123.
Teale, F. W. J. (1969) *Photochem. Photobiol. 10*, 363–374.
Thomas, D. D., & Hidalgo, C. (1978) *Proc. Natl. Acad. Sci. U.S.A. 75*, 5488–5492.
Thomas, D. D., Bigelow, D. J., Squier, T. C., & Hidalgo, C. (1982) *Biophys. J. 37*, 217–225.
Zannoni, C. (1981) *Mol. Phys. 42*, 1303–1320.

# Correlations between Reduction Potential, CO Stretch Frequency, and CO Half-Bandwidth in Hemoproteins†

M. L. Smith, J. Paul, P. I. Ohlsson, and K. G. Paul*

ABSTRACT: For 15 natural and artificial hemoproteins the Fe(III)/Fe(II) reduction potentials ($E_{m7}$) correlate linearily with the CO stretch frequencies ($\nu_{CO}$) and inversely with the half-bandwidths ($\Delta\nu_{1/2}$) of the carbonyl derivatives. Deviations from the correlation $E_{m7}/\nu_{CO}$ do occur as a sign of additional factors affecting $\nu_{CO}$. Thus, an aberrantly low $\nu_{CO}$ indicates hydrogen bonding of CO whereas aberrantly high values of four hemoproteins are discussed in terms of steric restraints upon CO. Horseradish peroxidase isoenzyme C was reconstituted with three and whale myoglobin with four artificial hemes, substituted at the 2,4-positions. For both sets of artificial hemoproteins, $\nu_{CO}$ responds to $E_{m7}$ in the same manner as for native hemoproteins. In the case of $\Delta\nu_{1/2}$, the covariation with $E_{m7}$ was less pronounced after substitution. Quantum mechanical Hartree–Fock–Slater-type calculations on a carbonylheme model ($N_5C_{14}Fe$·CO) show that $\nu_{CO}$ and $\Delta\nu_{1/2}$ respond to changes in total charge on carbonylheme, simulated by adding or withdrawing electrons from this model. The experimental correlations between $\nu_{CO}$ and $\Delta\nu_{1/2}$ with $E_{m7}$ are accounted for by a high density of states for metal-bound CO around the highest occupied and lowest unoccupied orbitals. The hydrogen bonding to CO found only with proteins of low $E_{m7}$ can be explained by the increase of negative charge upon the oxygen of CO with increasing negative charge upon carbonylheme. A pronounced decrease of $\Delta\nu_{1/2}$ was calculated for a Fe–C–O unit bent at 135° and a smaller decrease for a unit tilted 45° from heme normal. The increase in $\Delta\nu_{1/2}$ that accompanies an increase in space available to liganded CO and increased conformational randomness is discussed in terms of electron distribution and $E_m$.

In hemoproteins, the iron atom, porphyrin, protein moiety, and surrounding solvent form a balanced system that can engage in a variety of reactions with the transfer of two, one, or zero electrons. Most of these proteins carry protoheme; others carry heme A or C. The Fe(III)/Fe(II) reduction potential $E_m$[1] reflects the electronic structure of the iron atom and is hence a highly informative parameter. The $E_m$ values of protohemoproteins depend upon the protein moiety and span a range of about 0.5 V. Iron spin state and axial ligand strength may determine $E_m$ and the reactivity of a hemoprotein (Williams, 1961; Perutz, 1972; Moore & Williams, 1977), but this idea has met difficulties (Korszun et al., 1982). Another proposal is that $E_m$ is determined by the dielectric constant of the heme surroundings (Kassner, 1972). This proposal has been examined by Stellwagen (1978), who emphasized the importance of the extent of porphyrin exposure to solvent water. The replacement of the 2,4-vinyl groups of protoheme by other electron-redistributing groups affects not only $E_m$ of the hemoprotein (Yamada et al., 1975) but also biological functions such as the binding of $O_2$ to Hb and Mb (Makino & Yamazaki, 1974; Asakura et al., 1982) or the rate of reduction of peroxidase compound II by electron donors (Chance & Paul, 1960; Ohlsson & Paul, 1973).

Bound CO has extensively been used to probe the reactivity of metal atoms in copper proteins and hemoproteins and on metal surfaces, changes concerning CO being monitored by means of various vibrational spectroscopic methods. A compilation of values for $E_{m7}$ and $\nu_{CO}$ of five protohemoproteins and cytochrome $a_3$ indicated a linear covariation between $E_{m7}$ and $\nu_{CO}$ (Barlow et al., 1976). This study also showed that deviations from the linear correlation did occur in carbonyl-peroxidases and attributed them to the formation of a hydrogen bond between CO and the protein moiety. More limited correlations have been suggested between $\nu_{CO}$ and porphyrin $pK_3$ and $\nu_{NH}$ (Alben & Caughey, 1968), between $\nu_{CO}$ and $n$ log $P_{1/2}$ for $O_2$ binding (Berzofsky et al., 1972), and between

† From the Department of Physiological Chemistry, Umeå University, S-901 87 Umeå, Sweden (M.L.S., P.I.O., and K.G.P.), and the Department of Physics, Chalmers University of Technology, S-412 96 Göteborg, Sweden (J.P.). *Received December 12, 1983; revised manuscript received July 3, 1984.* This study was supported by the Swedish Medical Research Council with Grants B83-3X-6522 and B82-13R-6333.

[1] Abbreviations: Mb, myoglobin; Hb, hemoglobin; CTT, *Chironomous thummi thummi*; CCP, cytochrome *c* peroxidase; HRP, horseradish peroxidase; peroxidase, EC 1.11.1.7; IR, infrared; NMR, nuclear magnetic resonance; $\nu_{CO}$, stretch frequency of CO IR absorption band; $\Delta\nu_{1/2}$, half-bandwidth of CO IR absorption band; $E_m$, reduction potential; $E_{m7}$, $E_m$ at pH 7; Tris, tris(hydroxymethyl)aminomethane; EDTA, ethylenediaminetetraacetic acid.

0006-2960/84/0423-6776$01.50/0 